Laser beam steering for GRACE Follow-On intersatellite interferometry

Daniel Schütze,[1,*] Gunnar Stede,[1] Vitali Müller,[1] Oliver Gerberding,[1,3,4] Tamara Bandikova,[2] Benjamin S. Sheard,[1,5] Gerhard Heinzel,[1] and Karsten Danzmann[1]

[1]*Max Planck Institute for Gravitational Physics (Albert Einstein Institute) and Institute for Gravitational Physics, Leibniz Universität Hannover, Callinstr. 38, 30167 Hanover, Germany*
[2]*Institut für Erdmessung, Leibniz Universität Hannover, Schneiderberg 50, 30167 Hanover, Germany*
[3]*Now working at National Institute of Standards and Technology, Gaithersburg, Maryland 20899, USA*
[4]*Also working at Joint Quantum Institute, University of Maryland, College Park, Maryland 20741, USA*
[5]*Now working at Kayser-Threde GmbH, Munich, Germany*

[*]*Daniel.Schuetze@aei.mpg.de*

Abstract: The GRACE Follow-On satellites will use, for the first time, a *Laser Ranging Interferometer* to measure intersatellite distance changes from which fluctuations in Earth's geoid can be inferred. We have investigated the *beam steering method* that is required to maintain the laser link between the satellites. Although developed for the specific needs of the GRACE Follow-On mission, the beam steering method could also be applied to other intersatellite laser ranging applications where major difficulties are common: large spacecraft separation and large spacecraft attitude jitter. The beam steering method simultaneously coaligns local oscillator beam and transmitted beam with the laser beam received from the distant spacecraft using Differential Wavefront Sensing. We demonstrate the operation of the beam steering method on breadboard level using GRACE satellite attitude jitter data to command a hexapod, a six-degree-of-freedom rotation and translation stage. We verify coalignment of local oscillator beam/ transmitted beam and received beam of better than 10 µrad with a stability of 10 µrad/$\sqrt{\text{Hz}}$ in the GRACE Follow-On measurement band of 0.002...0.1 Hz. Additionally, important characteristics of the beam steering setup such as Differential Wavefront Sensing signals, heterodyne efficiency, and suppression of rotation-to-pathlength coupling are investigated and compared with analysis results.

© 2014 Optical Society of America

OCIS codes: (120.0120) Instrumentation, measurement, and metrology; (120.3180) Interferometry; (120.3940) Metrology; (120.4640) Optical instruments; (120.6085) Space instrumentation.

References and links

1. B. D. Tapley, S. Bettadpur, M. Cheng, D. Hudson, and G. Kruizinga, "Early results from the gravity recovery and climate experiment," in *Astrodynamics Specialist Conference*, J. D. Lafontaine, J. DeLafontaine, J. Treder, M. T. Soyka, and J. A. Sims, eds. (Astrodynamics, 2003), 1899–1911.
2. B. D. Tapley, S. Bettadpur, J. C. Ries, P. F. Thompson, and M. M. Watkins, "GRACE measurements of mass variability in the earth system," Science **305**, 503–505 (2004).

#217032 - $15.00 USD Received 15 Jul 2014; revised 29 Aug 2014; accepted 29 Aug 2014; published 25 Sep 2014
(C) 2014 OSA

3. B. D. Tapley, S. Bettadpur, M. Watkins, and C. Reigber, "The gravity recovery and climate experiment: Mission overview and early results," Geophys. Res. Lett. **31**, L09607 (2004).
4. B. D. Tapley, D. P. Chambers, S. Bettadpur, and J. C. Ries, "Large scale ocean circulation from the GRACE GGM01 Geoid," Geophys. Res. Lett. **30**, 2163 (2003).
5. R. Schmidt, F. Flechtner, U. Meyer, K.-H. Neumayer, C. Dahle, R. König, and J. Kusche, "Hydrological signals observed by the GRACE satellites," Surv. Geophys. **29**, 319–334 (2008).
6. B. Wouters, D. Chambers, and E. J. O. Schrama, "GRACE observes small-scale mass loss in Greenland," Geophys. Res. Lett. **35**, L20501 (2008).
7. V. M. Tiwari, J. Wahr, and S. Swenson, "Dwindling groundwater resources in northern India, from satellite gravity observations," Geophys. Res. Lett. **36**, L18401 (2009).
8. C. Dunn, W. Bertiger, Y. Bar-Sever, S. Desai, B. Haines, D. Kuang, G. Franklin, I. Harris, G. Kruizinga, T. Meehan, S. Nandi, D. Nguyen, T. Rogstad, J. B. Thomas, J. Tien, L. Romans, M. Watkins, S. C. Wu, S. Bettadpur, and J. Kim, "Instrument of GRACE: GPS augments gravity measurements," GPS World **14**, 16–28 (2003).
9. P. Touboul, E. Willemenot, B. Foulon, and V. Josselin, "Accelerometers for CHAMP, GRACE and GOCE space missions: Synergy and evolution," B. Geofis. Teor. Appl. **40**, 321–327 (1999).
10. M. van den Broeke, J. Bamber, J. Ettema, E. Rignot, E. Schrama, W. J. van de Berg, E. van Meijgaard, I. Velicogna, and B. Wouters, "Partitioning recent Greenland mass loss," Science **326**, 984–986 (2009).
11. B. S. Sheard, G. Heinzel, K. Danzmann, D. A. Shaddock, W. M. Klipstein, and W. M. Folkner, "Intersatellite laser ranging instrument for the GRACE follow-on mission," J. Geod. **86**, 1083–1095 (2012).
12. R. L. Ward, R. Fleddermann, S. Francis, C. Mow-Lowry, D. Wuchenich, M. Elliot, F. Gilles, M. Herding, K. Nicklaus, J. Brown, J. Burke, S. Dligatch, D. Farrant, K. Green, J. Seckold, M. Blundell, R. Brister, C. Smith, K. Danzmann, G. Heinzel, D. Schütze, B. S. Sheard, W. Klipstein, D. E. McClelland, and D. A. Shaddock, "The design and construction of a prototype lateral-transfer retro-reflector for inter-satellite laser ranging," Class. Quant. Grav. **31**, 095015 (2014).
13. D. Schütze, D. Farrant, D. A. Shaddock, B. S. Sheard, G. Heinzel, and K. Danzmann, "Measuring coalignment of retroreflectors with large lateral incoming-outgoing beam offset," Rev. Sci. Instrum. **85**, 035103 (2014).
14. D. Schütze, V. Müller, G. Stede, B. S. Sheard, G. Heinzel, K. Danzmann, A. J. Sutton, and D. A. Shaddock, "Retroreflector for GRACE follow-on: Vertex vs. point of minimal coupling," Opt. Express **22**, 9324–9333 (2014).
15. P. R. Yoder, "Study of light deviation errors in triple mirrors and tetrahedral prisms," J. Opt. Soc. Am. **48**, 496–499 (1958).
16. G. Hechenblaikner, "Measurement of the absolute wavefront curvature radius in a heterodyne interferometer," J. Opt. Soc. Am. A **27**, 2078–2083 (2010).
17. T. Schuldt, M. Gohlke, D. Weise, U. Johann, A. Peters, and C. Braxmaier, "Picometer and nanoradian optical heterodyne interferometry for translation and tilt metrology of the LISA gravitational reference sensor," Class. Quant. Grav. **26**, 085008 (2009).
18. H. I. Campbell and A. H. Greenaway, "Wavefront sensing: From historical roots to the state-of-the-art," EAS Publ. **22**, 165–185 (2006).
19. G. Heinzel, A. Rüdiger, R. Schilling, K. Strain, W. Winkler, J. Mizuno, and K. Danzmann, "Automatic beam alignment in the Garching 30-m prototype of a laser-interferometric gravitational wave detector," Opt. Commun. **160**, 321–334 (1999).
20. E. Morrison, B. J. Meers, D. I. Robertson, and H. Ward, "Automatic alignment of optical interferometers," Appl. Opt. **33**, 5041–5049 (1994).
21. D. Z. Anderson, "Alignment of resonant optical cavities," Appl. Opt. **23**, 2944–2949 (1984).
22. C. Mahrdt, Max-Planck-Institute for Gravitational Physics (Albert Einstein Institute) and Institute for Gravitational Physics, Leibniz Universität Hannover, Callinstr. 38, 30167 Hanover, Germany, is preparing a manuscript to be called "Initial line-of-sight calibration for the GRACE follow-on laser ranging interferometer."
23. D. A. Shaddock, B. Ware, P. G. Halverson, R. E. Spero, and B. Klipstein, "Overview of the LISA phasemeter," AIP Conf. Proc. **873**, 689–696 (2006).
24. I. Bykov, J. J. E. Delgado, A. F. García Marín, G. Heinzel, and K. Danzmann, "LISA phasemeter development: Advanced prototyping," J. Phys. Conf. Ser. **154**, 012017 (2009).
25. O. Gerberding, B. S. Sheard, I. Bykov, J. Kullmann, J. J. E. Delgado, K. Danzmann, and G. Heinzel, "Phasemeter core for intersatellite laser heterodyne interferometry: modelling, simulations and experiments," Class. Quant. Grav. **30**, 235029 (2013).
26. D. Fink, "Coherent detection signal-to-noise," Appl. Opt. **14**, 689–690 (1975).
27. E. D. Fitzsimons, J. Bogenstahl, J. Hough, C. J. Killow, M. Perreur-Lloyd, D. I. Robertson, and H. Ward, "Precision absolute positional measurement of laser beams," Appl. Opt. **52**, 2527–2530 (2013).
28. Helmholtz Centre Potsdam – GFZ German Research Centre for Geosciences, http://isdc.gfz-potsdam.de.
29. National Aeronautics and Space Administration (NASA)/ Jet Propulsion Laboratory (JPL), http://podaac.jpl.nasa.gov.
30. T. Bandikova, J. Flury, and U.-D. Ko, "Characteristics and accuracies of the GRACE inter-satellite pointing," Adv. Space Res. **50**, 123–135 (2012).

#217032 - $15.00 USD Received 15 Jul 2014; revised 29 Aug 2014; accepted 29 Aug 2014; published 25 Sep 2014
(C) 2014 OSA

1. Introduction

Since the *Gravity Recovery and Climate Experiment* (GRACE, see e.g. [1–3]) was launched in 2002, it has been successfully monitoring the spatial and temporal variations of Earth's geoid, proving the feasibility of low-orbit satellite-to-satellite tracking. In particular, changes in the gravitational potential caused by hydrological mass transport could be studied in detail [4–7].

GRACE consists of two identical satellites in a common, freely decaying, low polar orbit. Occasional orbit maneuvers keep the satellite separation between 170–270 km with relative spacecraft velocities of a few m/s. Intersatellite distance changes are measured with micrometer accuracy using a *microwave ranging system*. From the measured distance changes, the gravity potential of Earth can be derived [8].

Non-gravitational forces caused by, e.g., atmospheric drag, solar radiation pressure, and Earth's albedo are removed from the measurements using an accelerometer [9]. Every month, sufficient coverage of the surface of the Earth is accumulated to yield an update of the gravity field. This makes it possible to study temporal changes in Earth's gravity field and to observe longterm trends, e.g. for testing climate models [10].

The GRACE Follow-On mission is to be launched in 2017 to continue these Earth gravity field measurements. In addition to the mircowave ranging system, GRACE Follow-On will utilize a *Laser Ranging Interferometer* (LRI, [11]) as technology demonstrator. The goal of the LRI is to improve the intersatellite distance measurements by more than one order of magnitude and to demonstrate the feasibility of laser interferometry for future geodesy missions based on high precision intersatellite ranging.

While the research presented in this paper focuses on LRI breadboard models, in parallel engineering models have been built by the industrial prime contractor (SpaceTech GmbH Immenstaad, STI). In June 2014, the LRI has passed the Critical Design Review and has thus entered the phase of flight unit production.

Figure 1 depicts the LRI concept, which is identical for both spacecraft. The LRI employs an *active receiver-transponder principle*. This means that the weak incoming RX beam is "amplified" by a strong local oscillator (LO) beam which is sent back to the distant spacecraft via retroreflection by the *Triple Mirror Assembly* (TMA, [12–14]). Due to local spacecraft attitude jitter, a *beam steering method* becomes necessary so that RX beam and LO beam remain coaligned and the TX beam reaches the distant spacecraft.

Since in GRACE Follow-On, the line-of-sight between the two spacecraft's (S/C) centers-of-masses (CM) will be occupied by the main science instrument, the microwave ranging system, and tanks of the cold gas propulsion system, an off-axis configuration had to be chosen in which the interferometer beams are routed using the Triple Mirror Assembly (TMA), which functions as a passive retroreflector [15]. By placing the TMA vertex at the S/C CM, virtually, distance changes between the two S/C centers-of-masses are measured and, additionally, rotation-to-pathlength couplings are cancelled, in the ideal case, due to the TMA properties [11, 14].

During the development of the LRI it turned out that this "racetrack" configuration allows for a simple implementation of closed-loop beam steering, which maximizes the interferometric contrast and ensures at the same time TX beam pointing towards the distant satellite due to the special properties of the TMA. To our knowledge, on-axis concepts have not shown such a simple capability of closed-loop beam steering. For this reason, we would now consider the "racetrack" configuration a promising candidate architecture even for a new mission design in which the line-of-sight would be available.

The RX beam that is received from the distant spacecraft is clipped at an aperture on the LRI optical bench and then overlapped with the local oscillator (LO) beam on a beam splitter (BS, nominally 90% reflective, 10% transmissive). The LO beam from the local oscillator

#217032 - $15.00 USD Received 15 Jul 2014; revised 29 Aug 2014; accepted 29 Aug 2014; published 25 Sep 2014
(C) 2014 OSA

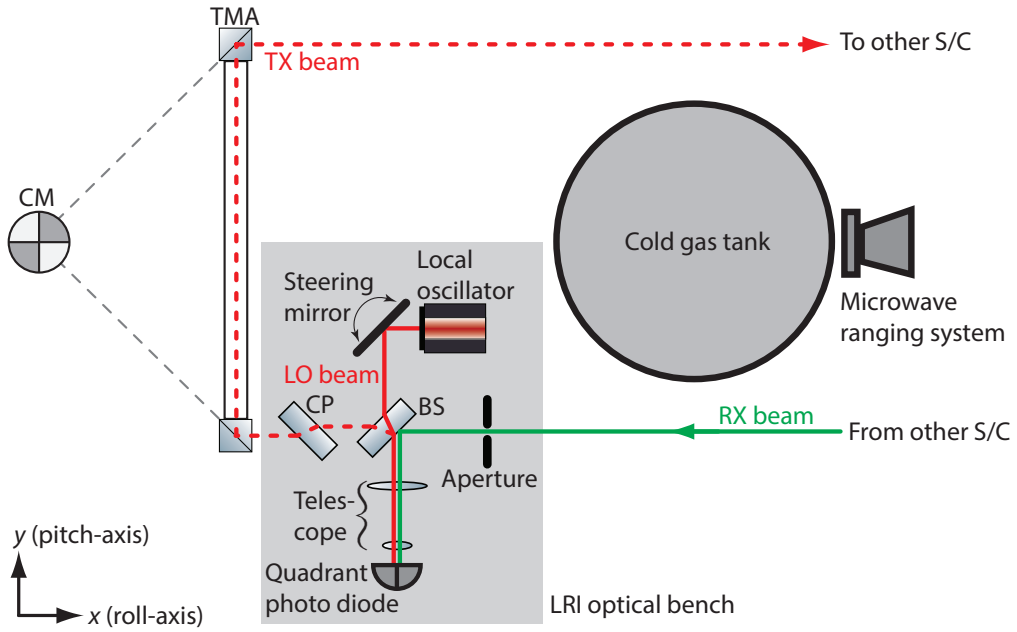

Fig. 1. Sketch of Laser Ranging Interferometer (LRI) on one of the two identical GRACE Follow-On spacecraft (S/C). The Triple Mirror Assembly (TMA) routes the beam around the cold gas tank and the microwave ranging system. The TMA vertex is located at the S/C center-of-mass (CM). On the LRI optical bench, LO beam and RX beam are interfered on a beam splitter (BS) and imaged on a quadrant photo diode (QPD) using a telescope. On the QPD, both integrated phase and relative beam tilt are measured using Differential Wavefront Sensing (DWS). By zeroing the DWS singals in closed-loop, the steering mirror keeps LO beam and RX beam coaligned such that the outgoing TX beam that has been retroreflected by the TMA is sent back to the distant satellite. The compensation plate (CP) cancels linear rotation-to-pathlength coupling that is caused by the beam splitter (BS).

laser, which serves both as LO beam and TX beam source, is guided over a 2-axes steering mirror. Both steering mirror surface (more specifically, the point where the beam is incident) and aperture plane are simultaneously imaged on a quadrant photo diode (QPD) using a 2-lens telescope. The telescope suppresses diffraction effects caused by beam clipping at the aperture and beamwalk due to local spacecraft tilt. Furthermore, it reduces the beam sizes to match the QPD diameter.

On the QPD, both integrated phase and relative beam tilt between LO beam and RX beam are measured using Differential Wavefront Sensing (DWS, [16–21]). The integrated phase contains the intersatellite ranging information, whereas the DWS signals are minimized in closed-loop using the steering mirror. By this, simultaneous coalignment of LO beam/ TX beam and RX beam under local spacecraft attitude jitter is achieved.

The LO beam that is reflected at the beam splitter (BS) passes through a *compensation plate* (CP) which cancels, in first order, local spacecraft rotation-to-pathlength coupling caused by the beam splitter [11]. Finally, the TMA retroreflects the LO beam to send it back to the distant spacecraft (TX beam).

Right after launching the satellites into orbit, there will be an unknown offset on each spacecraft between the LRI optical axes and the startracker-derived spacecraft orientations. Furthermore, there will be an unknown offset between the laser frequencies on both spacecraft,

#217032 - $15.00 USD Received 15 Jul 2014; revised 29 Aug 2014; accepted 29 Aug 2014; published 25 Sep 2014
(C) 2014 OSA

which might be beyond the bandwidth of the QPDs. These offsets need to be calibrated during an initial comissioning scan. While the steering mirrors on both spacecraft perform angular scan patterns, the laser frequency on one spacecraft ("slave") is tuned to find the steering mirror positions for each spacecraft and the laser frequency on the slave spacecraft that produce the largest heterodyne signal amplitude [22].

2. Measurement setup

We present the setup shown in Fig. 2 to test the beam steering method for the GRACE Follow-On LRI. This setup comprises an *optical bench breadboard model* (OBBM) which incorporates all functionalities of the LRI optical bench.

The OBBM is installed on a six-degree-of-freedom hexapod stage (PI GmbH & Co. KG, M824, 500 nm positional and 6 µrad rotational repeatability by specification) which can be commanded to perform calibrated translations and rotations around specified pivots. We have used this setup to verify closed-loop beam steering under realistic satellite attitude jitter.

2.1. Laser beam generation

The GRACE Follow-On LRI uses heterodyne interferometry to track intersatellite distance changes. To this end, the laser beams with wavelength of 1064 nm generated on the two spacecraft need to be offset phase-locked, with one of the spacecraft operating as master, the other as slave.

The intersatellite ranging information can only be unambiguous if the Doppler frequency shifts incurred due to relative spacecraft motion stay below the offset frequency of the phase-lock. Since the intersatellite velocities are a few m/s, an offset frequency of several MHz is required.

Furthermore, due to the large spacecraft separation of 200 km, the RX beam that is received by the local spacecraft, cf. Fig. 1, has expanded to a radius of 30 m producing a *flattop beam profile* with flat wavefront and flat intensity distribution on the 8 mm diameter aperture of the LRI optical bench.

We now describe how we produce the required laser beams for our setup in Fig. 2. The laser beams are generated by two offset phase-locked Mephisto 500 lasers (Innolight GmbH) at 1064 nm with an offset frequency of 6.25 MHz and delivered to the setup with optical fibers.

The RX beam that needs to be flat in both phase and intensity profile is produced with the *RX beam generator* which consists of an open fiber end adjusted to the focal point of an aspherical lens with 200 mm focal length (Thorlabs, AL100200-C). We have aligned the fiber end with respect to the lens while observing the beam leaving the RX beam generator with a Shack-Hartmann sensor (Imagine Optics S.A., HASO3-128-GE2). The generated RX beam has a diameter of 2 cm over which the wavefront varies with peak-to-valley of 440 nm. Over the 8 mm OBBM aperture, the RX beam exhibits a peak-to-valley wavefront error of 160 nm and an intensity drop of 20%. Generation of a beam with smaller wavefront error and less intensity drop would be possible with increased effort, yet this was not deemed necessary within the scope of this investigation.

The LO beam is delivered by the *LO beam generator* which consists of a commercial fiber collimator (Schäfter&Kirchhoff, 69FC-4-A11-03) and a 2-lens telescope (lenses: Thorlabs Inc., LA1027-C and LA1509-C) to shape the beam. We have adjusted the LO beam generator while monitoring the generated beam with a Shack-Hartmann sensor. A Gaussian beam with 4.6 mm Gaussian waist diameter and a flat wavefront with 117 nm peak-to-valley wavefront error on the steering mirror (SM) surface (nominal waist position) is produced.

#217032 - $15.00 USD Received 15 Jul 2014; revised 29 Aug 2014; accepted 29 Aug 2014; published 25 Sep 2014
(C) 2014 OSA

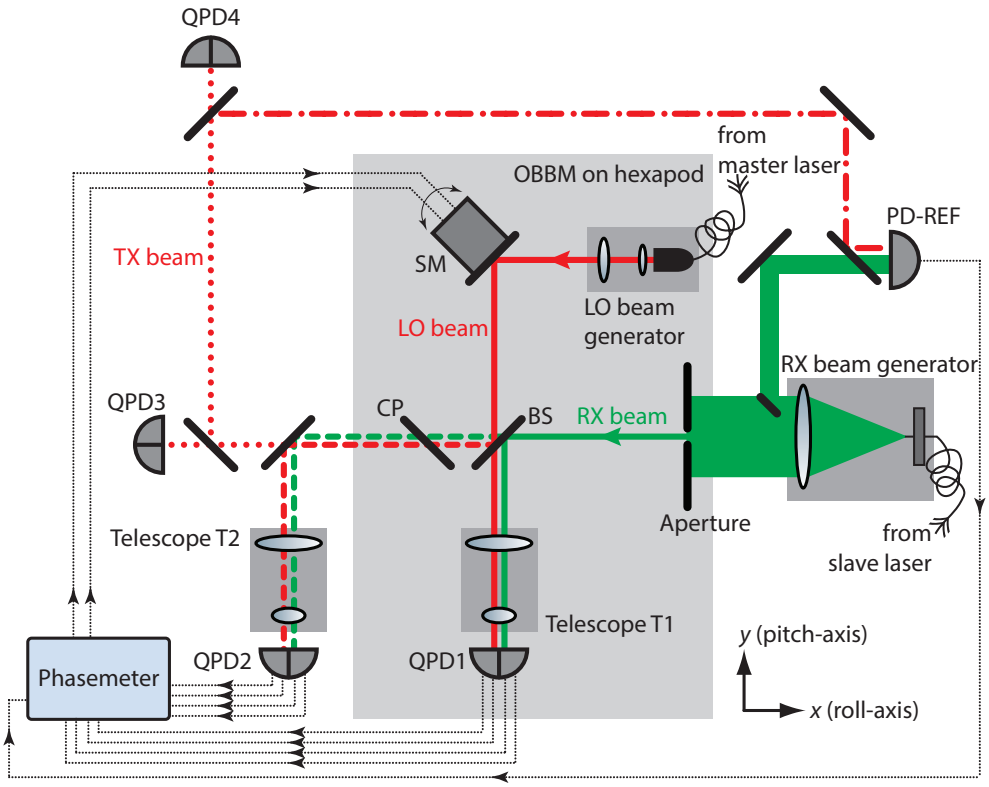

Fig. 2. Setup to verify the closed-loop beam steering method of the optical bench breadboard model (OBBM) mounted on a hexapod. The slave laser is offset phase-locked to the master laser. LO beam and RX beam are delivered to the setup via optical fibers and interfered on a beam splitter (BS). At one port of BS, the beams (solid lines) are imaged on quadrant photo diode QPD1 with telescope T1. The phases of the four QPD1 segments are recorded using a digital phasemeter. This phasemeter also calculates the Differential Wavefront Sensing (DWS) signals which can be fed back in closed-loop to the steering mirror (SM). At the second port of BS, the reflected LO beam and the transmitted RX beam (dashed lines) pass the compensation plate (CP). After leaving the OBBM, LO beam and RX beam are imaged on QPD2 using telescope T2. The DWS signals obtained from QPD2 give an out-of-loop confirmation of LO beam and RX beam coalignment during SM closed-loop operation. Furthermore, orientation changes of the TX beam (dotted line) can be inferred from two calibrated position-sensitive quadrant photo diodes QPD3 and QPD4. To investigate OBBM rotation-to-pathlength coupling, a part of the RX beam is diverted before entering the OBBM and inferfered with the TX beam (dot-dashed line) on the single-element photo diode PD-REF to obtain an interferometric reference measurement.

#217032 - $15.00 USD Received 15 Jul 2014; revised 29 Aug 2014; accepted 29 Aug 2014; published 25 Sep 2014
(C) 2014 OSA

2.2. *Differential wavefront sensing signals, closed-loop beam steering, and heterodyne efficiency*

The information on relative LO beam and RX beam tilt that is required for the beam steering method is obtained by Differential Wavefront Sensing (DWS). We now explain how the DWS signals are generated in our setup (Fig. 2) using a *digital phasemeter*, how they can be fed back to the steering mirror in closed-loop, and how they can be calibrated to obtain the desired information on relative LO beam and RX beam tilts. Furthermore, we introduce the *heterodyne efficiency*, which describes how well LO beam and RX beam overlap.

Following the beam path in Fig. 2, both LO beam and RX beam are interfered on a 95% reflective beam splitter (BS). At one port of the beam splitter, both beams (solid lines) are imaged on a quadrant photo diode (QPD1) with telescope T1 consisting of two spherical lenses with focal lengths of 80 mm and 10 mm (Linos/Qioptiq GmbH & Co. KG, G311712000 and G311026000). The telescope has been designed for an image size demagnification of 1/8 to adapt the beam sizes to the QPD1 diameter of 1 mm.

Telescope T1 simultaneously images the steering mirror surface and the aperture plane to minimize diffraction effects of the RX beam caused by clipping at the aperture and beamwalk of the RX beam due to hexapod rotations (i.e., local satellite rotations during the actual mission) and of the LO beam due to steering mirror tilts. The position of QPD1 along the beams is adjusted to coincide with the image plane of telescope T1 by performing steering mirror (SM, PI GmbH & Co. KG, S-325.3SD, with controller E-616.S0G) tilts and minimizing beamwalk of the LO beam on QPD1 down to 2 µm/mrad, which was limited by the noise floor of the adjustment. During the actual mission, maximum tilts are expected to be a few mrad.

As QPD1, we use the Elegant Breadboard Model of the GRACE Follow-On quadrant photo receiver with an InGaAs quadrant photo diode (OSI Optoelectronics AS, FCI-InGaAs-Q1000), which was kindly provided by "Deutsches Zentrum für Luft- und Raumfahrt" (DLR). The signals from the four QPD1 quadrants A1, B1, C1, D1 (quadrant naming convention: A top left, B top right, C bottom left, D bottom right) are processed using an in-house built *digital phasemeter*.

The phasemeter is a variant of the readout system originally developed for the space-based gravitational wave detector LISA [23, 24]. A schematic overview of the phasemeter (PM) architecture which has been realized within a field-programmable gate array (FPGA) is shown in Fig. 3.

The analogue photo receiver signals from the four QPD1 quadrants $i = \mathrm{A1}, \mathrm{B1}, \mathrm{C1}, \mathrm{D1}$ are digitized using analogue-to-digital converters (ADCs) with a sampling rate of 40 MHz and then fed into digital phase-locked loops (PLLs), which determine the frequency f_i, amplitude I_i, and phase φ_i of each QPD1 quadrant [25]. The phases φ_i are combined appropriately to obtain DWS signals for horizontal ($\mathrm{DWS1_{hor}}$) and vertical ($\mathrm{DWS1_{ver}}$) relative beam tilts between LO beam and RX beam (in Fig. 3, only the generation of $\mathrm{DWS1_{hor}}$ is shown):

$$\begin{aligned} \mathrm{DWS1_{hor}} &= 0.5 \cdot (\varphi_{\mathrm{A1}} + \varphi_{\mathrm{C1}} - \varphi_{\mathrm{B1}} - \varphi_{\mathrm{D1}}), \\ \mathrm{DWS1_{ver}} &= 0.5 \cdot (\varphi_{\mathrm{A1}} + \varphi_{\mathrm{B1}} - \varphi_{\mathrm{C1}} - \varphi_{\mathrm{D1}}). \end{aligned} \tag{1}$$

The DWS signals $\mathrm{DWS1_{hor}}$ and $\mathrm{DWS1_{ver}}$ are fed through a single integrator ("Servo"), acting as servo controller of the steering mirror loop. The gain of the steering mirror loop is controlled via simple bit shifting. The resulting actuator signal is fed to the steering mirror electronics via digital-to-analogue converters (DACs). The actuation axes of the steering mirror are well-aligned to the DWS1/ QPD1 axes within a few degrees, therefore no additional rotation matrix

#217032 - $15.00 USD Received 15 Jul 2014; revised 29 Aug 2014; accepted 29 Aug 2014; published 25 Sep 2014
(C) 2014 OSA

calculation is necessary.

The gain of the steering mirror loop is set using a simple control model, including the simulated DWS coupling factor (see below, Eqs. (2) and (4)), the optical geometry, the steering mirror gain, and the digital signal processing.

The DWS signals $\mathrm{DWS1_{hor}}$ and $\mathrm{DWS1_{ver}}$ from Eq. (1) can be calibrated to relative beam tilt

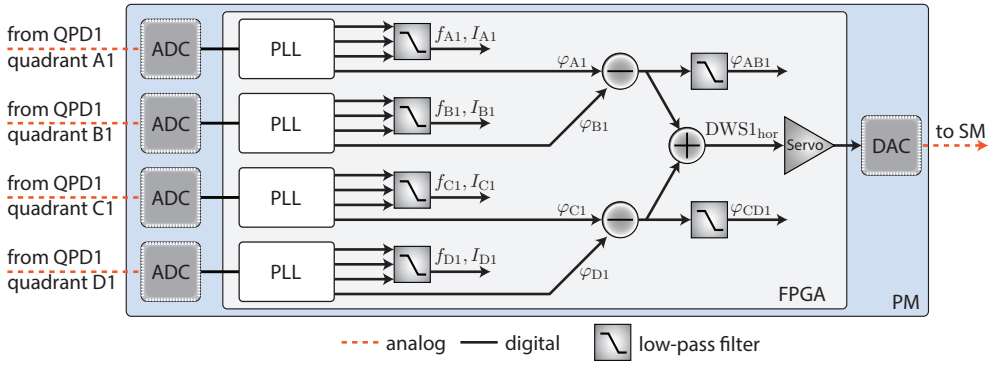

Fig. 3. Schematic overview of the phasemeter (PM) architecture embedded within a field-programmable gate array (FPGA). Shown is the readout of frequency f_i, amplitude I_i, and phase φ_i, $i = \mathrm{A1, B1, C1, D1}$, of the four QPD1 quadrants via digital phase-locked loops (PLLs) and the generation of the DWS signal $\mathrm{DWS1_{hor}}$ according to Eq. (1). The DWS signal is then passed on to an integrator which acts as servo controller of the steering mirror loop. The resulting actuator signal is fed to the steering mirror (SM) electronics via digital-to-analogue converters (DACs).

angles by performing calibrated hexapod rotations θ_{yaw} around the z-axis and θ_{pitch} around the y-axis (coordinate frame depicted in Fig. 2). The relation between hexapod rotations and DWS signals is given by the DWS transfer matrix M1,

$$\begin{pmatrix} \mathrm{DWS1_{hor}} \\ \mathrm{DWS1_{ver}} \end{pmatrix} = \begin{pmatrix} \mathrm{M1_{11}} & \mathrm{M1_{12}} \\ \mathrm{M1_{21}} & \mathrm{M1_{22}} \end{pmatrix} \begin{pmatrix} \theta_{\mathrm{yaw}} \\ \theta_{\mathrm{pitch}} \end{pmatrix}. \tag{2}$$

The unit of M1 is rad/rad converting relative geometric wavefront tilt between LO beam and RX beam at the beam splitter (BS) to DWS electrical phase. The diagonal elements of M1, $\mathrm{M1_{11}}$ and $\mathrm{M1_{22}}$, should be dominant relating hexapod yaw rotations to horizontal beam tilt and pitch rotations to vertical beam tilt. The off-diagonal elements of M1, $\mathrm{M1_{12}}$ and $\mathrm{M1_{21}}$, arise from misalignments between the hexapod coordinate frame shown in Fig. 2 and the quadrants of QPD1.

An important characteristic of the OBBM setup is the *heterodyne efficiency* γ [26] of the interfering beams, which is a measure of how well LO beam and RX beam overlap. The heterodyne efficiency determines the obtainable signal amplitude and its dependency on relative beam tilts. It is of particular interest to estimate the appropriate parameters for simulations of the critical initial commissioning scan mentioned in Sec. 1, during which the unknown satellite attitude offsets with respect to the line-of-sight are calibrated [22]. For each QPD1 segment, we can determine the heterodyne efficiency γ from the directly measurable interferometric contrast c,

$$\gamma = \frac{c^2}{4} \frac{(P_{\mathrm{LO}} + P_{\mathrm{RX}})^2}{P_{\mathrm{LO}} P_{\mathrm{RX}}}. \tag{3}$$

Here, P_{LO} and P_{RX} are the light power of LO beam and RX beam respectively, incident on the QPD1 segments. The contrast c is given by the maximum and minimum light power

#217032 - $15.00 USD Received 15 Jul 2014; revised 29 Aug 2014; accepted 29 Aug 2014; published 25 Sep 2014
(C) 2014 OSA

levels $P_{\max}$ and $P_{\min}$ on the QPD1 segments due to the interference of the two beams, $c = (P_{\max} - P_{\min}) / (P_{\max} + P_{\min})$.

2.3. *Simulation of DWS signals and heterodyne efficiency*

We have numerically simulated the interference of LO beam and RX beam on QPD1 under hexapod pitch and yaw rotations using the specific parameters of our setup (Fig. 2): Gaussian LO beam with 4.6 mm waist diameter, flattop RX beam with 8 mm diameter, telescope T1 with 1/8 demagnification, QPD1 active area of 1 mm diameter, and QPD1 slit width of 44 µm (QPD1 dimensions determined with an optical microscope). For the simulation, perfect alignment of QPD1 quadrants and hexapod coordinates is assumed, so that the off-diagonal elements of the DWS transfer matrix M1 in Eq. (2) are zero and $\mathrm{M1}_{11}^{\mathrm{sim}} = -\mathrm{M1}_{22}^{\mathrm{sim}}$. Furthermore, flat LO beam and RX beam wavefronts were assumed and a flat RX beam intensity profile.

The simulations have been performed with Matlab®. On a 512×512 grid covering the QPD1 active area, the Gaussian LO beam wavefront was generated. For the RX beam, flattop wavefronts were generated with horizontal and vertical tilts ranging from $-550 \ldots 550$ µrad with 10 µrad step size. Each RX beam wavefront was then interfered with the LO beam wavefront. By integrating over each QPD1 segment, we have obtained the phases φ_i and the interferometric contrast c_i, $i = \mathrm{A1}, \mathrm{B1}, \mathrm{C1}, \mathrm{D1}$, for each segment.

With our simulations, we have calculated DWS signals according to Eq. (1). The simulation results are shown in Fig. 4. We have determined the DWS transfer matrix $\mathrm{M1}^{\mathrm{sim}}$ with Eq. (2) for small pitch and yaw angles inside the linear region outside of which phase wrapping occurs. The simulation yields

$$\mathrm{M1}_{11}^{\mathrm{sim}} = -\mathrm{M1}_{22}^{\mathrm{sim}} = 15,600\,\mathrm{rad/rad}. \tag{4}$$

In a next step, we have used our simulation to calculate the heterodyne efficiency of LO

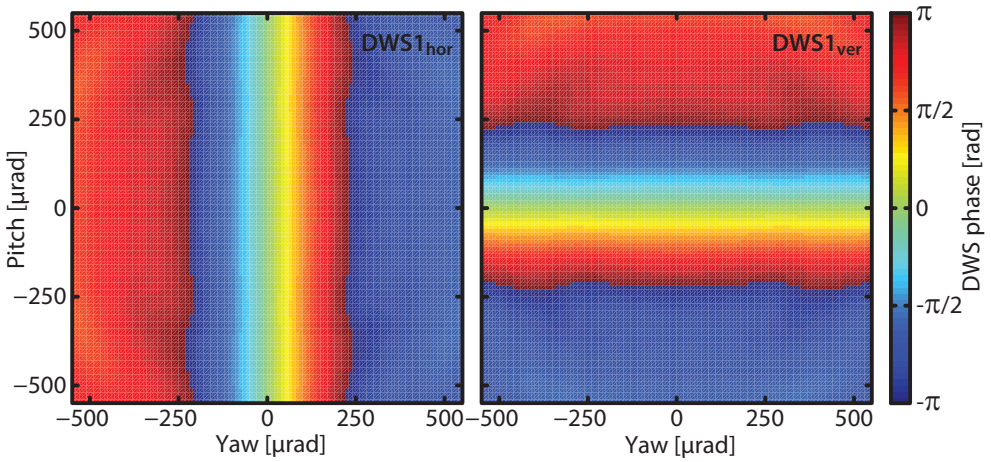

Fig. 4. Numerically simulated DWS signals $\mathrm{DWS1}_{\mathrm{hor}}$ (left) for horizontal and $\mathrm{DWS1}_{\mathrm{ver}}$ (right) for vertical relative beam tilts between LO beam and RX beam on QPD1 under hexapod pitch and yaw rotations.

beam and RX beam according to Eq. (3). The heterodyne efficiency for the simulated hexapod pitch and yaw rotations is displayed in Fig. 5 for the four QPD1 segments. For perfectly aligned LO beam and RX beam and the parameters of our setup, the simulated heterodyne efficiency for each quadrant reaches a maximum value of

$$\gamma_{\max}^{\mathrm{sim}} = 60\%. \tag{5}$$

#217032 - $15.00 USD Received 15 Jul 2014; revised 29 Aug 2014; accepted 29 Aug 2014; published 25 Sep 2014
(C) 2014 OSA

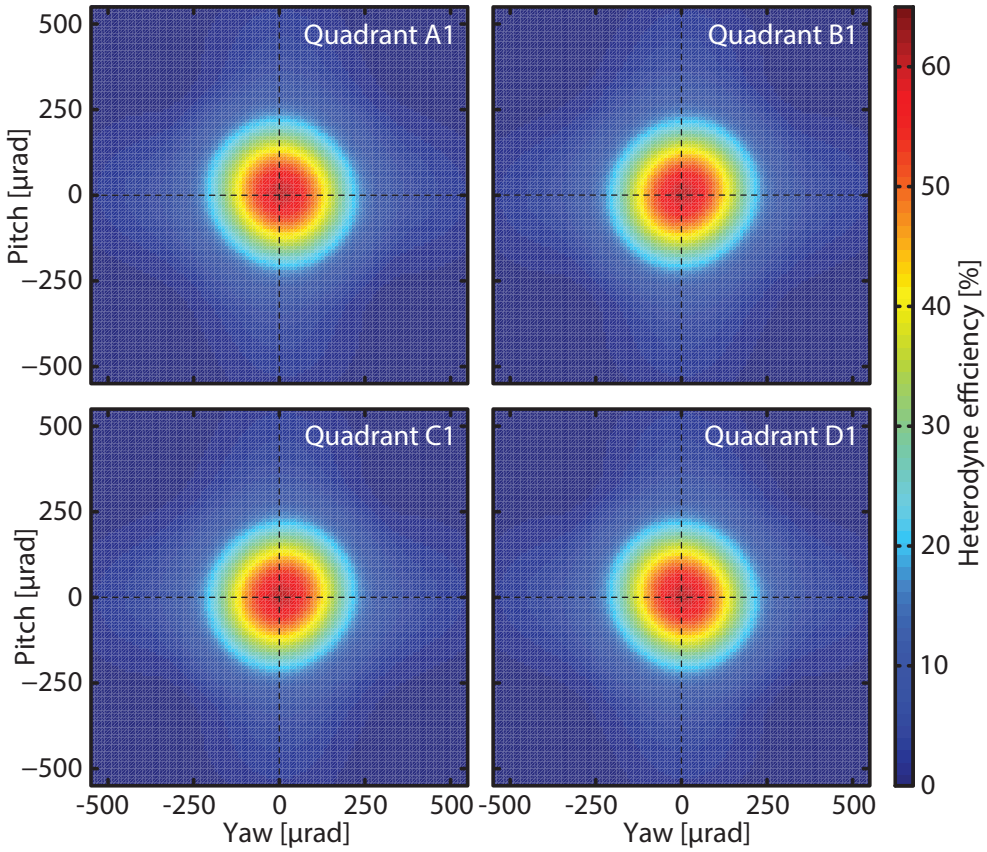

Fig. 5. Numerically simulated heterodyne efficiency of LO beam and RX beam on the four segments of QPD1 under hexapod pitch and yaw rotations. For perfectly aligned LO beam and RX beam and the parameters of our setup, the heterodyne efficiency on each QPD1 segment reaches a maximum value of 60%.

2.4. Coalignment of LO beam and RX beam

We want to test the OBBM beam steering method under realistic local spacecraft jitter which is simulated in our setup (Fig. 2) with a hexapod platform. To fulfill the LRI beam coalignment error budget, the coalignment error between LO beam and RX beam should be below 10 µrad with a stability of 10 µrad/$\sqrt{\text{Hz}}$ in the GRACE Follow-On frequency band of 0.002...0.1 Hz. To verify this requirement, we need to measure the coalignment of LO beam and RX beam with sufficient accuracy.

One could argue that the beam coalignment is readily available from the DWS signals obtained from QPD1. Yet since the DWS signals from QPD1 are minimized in closed-loop, all we see is the inherent closed-loop suppression. Thus to verify that LO beam and RX beam are coaligned during steering mirror closed-loop operation, an *out-of-loop* coalignment measurement is necessary. We now explain how this out-of-loop coalignment measurement is implemented in our setup.

At the second port of the beam splitter (BS, Fig. 2), reflected LO beam and transmitted RX beam (dashed lines) pass the compensation plate (CP). During the actual satellite mission, the

#217032 - $15.00 USD Received 15 Jul 2014; revised 29 Aug 2014; accepted 29 Aug 2014; published 25 Sep 2014
(C) 2014 OSA

transmitted RX beam is very weak in light power and can be neglected. In our setup, however, we have adjusted light powers as to further investigate both reflected LO beam and transmitted RX beam.

After leaving the OBBM, LO beam and RX beam are imaged on QPD2 using telescope T2 with spherical lenses of focal lengths 750 mm and 100 mm (Thorlabs Inc., LA1978-C and LA1509-C). The focal lengths were chosen such that a demagnification of roughly 1/8 is achieved while imaging both the steering mirror (SM) surface and the aperture plane on QPD2. QPD2 is an in-house built quadrant photo receiver with a 1 mm diameter InGaAs quadrant photo diode (Hamamatsu Photonics K.K., G6849-01) the phases of which are also recorded using the phasemeter.

For QPD2, DWS signals $DWS2_{hor}$, $DWS2_{ver}$ and DWS transfer matrix M2 are defined analogously to Eqs. (1) and (2). The DWS signals obtained from QPD2 can be used to validate LO beam and RX beam coalignment during steering mirror closed-loop operation.

Furthermore, measurements of the TX beam axis orientation (dotted line) are performed on two calibrated position-sensitive quadrant photo diodes QPD3 and QPD4. The power of the transmitted RX beam on QPD3, QPD4 is much smaller than the power of the TX beam so that it does not affect the measurements.

The QPDs are calibrated in a way that TX beam axis orientation changes can be inferred from differential position measurements between QPD3 and QPD4 [27]. Horizontal orientation changes are referred to as TX_{hor}, vertical orientation changes as TX_{ver}.

Since during cosed-loop beam steering, the TX beam should not change its orientation, this differential position measurement gives an additional validation of closed-loop beam steering operation with a DWS-independent measurement method; yet it only provides information on LO beam and RX beam coalignment *changes*.

2.5. Rotation-to-pathlength coupling

The pathlength through the beam splitter (BS) on the LRI optical bench (Fig. 1) is angle dependent. This leads to a large linear term in local spacecraft yaw rotation-to-pathlength coupling of 2.2 µm/mrad, which is cancelled by use of the compensation plate (CP, [11]). In the expected satellite attitude jitter range of several mrad, all remaining rotation-to-pathlength couplings should be smaller than 10 nm/mrad for roll and 80 nm/mrad for pitch and yaw to fulfill the LRI ranging error budget.

To demonstrate the cancellation of the large linear rotation-to-pathlength coupling from the beam splitter (BS) by use of a compensation plate (CP), and to show that all remaining rotation-to-pathlength couplings are sufficiently small, we have measured rotation-to-pathlength coupling of the OBBM system in Fig. 2. To accomplish this, an interferometric reference measurement is required to emulate the roundtrip measurement of the GRACE Follow-On LRI. To this end, a part of the RX beam is branched off before entering the OBBM and interfered with the TX beam, which is bypassing the OBBM (dot-dashed line), on a single-element photo diode, PD-REF.

3. Measurement results

3.1. Calibration of QPD phase offsets

Different delay times in the electronics lead to phase offsets between the quadrants of the QPDs. According to Eq. (1), those relative phase offsets couple directly into the DWS measurement. This is why calibration of phase offsets between the QPD segments is essential.

We have calibrated electronic phase offsets between the QPD segments for QPD1, QPD2 by amplitude-modulating the LO beam, Fig. 2, with a fiber-coupled amplitude modulator (Jenoptik AG, AM 1064), while the RX beam was being blocked. This emulates an interference beatnote

#217032 - $15.00 USD Received 15 Jul 2014; revised 29 Aug 2014; accepted 29 Aug 2014; published 25 Sep 2014
(C) 2014 OSA

with equal phase on all four QPD segments so that relative phase offsets between the quadrants can be inferred.

Phase offsets were calibrated to below 1 mrad with a stability of better than 100 µrad/$\sqrt{\text{Hz}}$ under ambient conditions in the GRACE Follow-On measurement frequency band of 0.002...0.1 Hz. With the expected DWS transfer matrix entries from Eq. (4), $\text{M1}_{11}^{\text{sim}} = -\text{M1}_{22}^{\text{sim}} = 15,600$ rad/rad, this corresponds to a relative LO beam and RX beam tilt error of less than 0.1 µrad, which is negligible.

After calibration, the phase offsets were subtracted in the phasemeter signal processing chain.

3.2. Measurement of DWS transfer matrix and heterodyne efficiency

Using our setup shown in Fig. 2, we have performed calibrated hexapod rotations around the *y*-axis (pitch) and the *z*-axis (yaw) with open steering mirror loop; thus the steering mirror was fixed at its nominal zero position. The center of the OBBM aperture was chosen as nominal pivot for the hexapod rotations to prevent walking transversially over the RX beam plane.

During hexapod rotations, we have recorded the DWS signals and the heterodyne efficiency. The DWS signals obtained from QPD1 as function of hexapod pitch and yaw rotations are shown in Fig. 6. The results for QPD2 are very similar to the results obtained for QPD1.

The behavior of the measured DWS signals with hexapod pitch and yaw rotations is very similar to the simulated behavior from Fig. 4: There is a linear response of DWS signals to pitch and yaw up to roughly 200 µrad, and then phase wrapping occurs. While a concentric ring structure can be seen both in the simulation Fig. 4 and in the measurement Fig. 6 outside of the linear region, the phase fluctuations that it causes are more deeply indented in the measurement and even cross through zero. This is not fully understood, but might be caused by the non-flatness of LO beam and RX beam wavefront, cf. Sec. 2.1. However, for the actual satellite mission, only the region within ± 100 µrad relative beam tilt is of interest, since for larger relative LO beam and RX beam tilts, the heterodyne signal amplitudes drop below the noise level.

The DWS transfer matrices M1, M2 (cf. Eq. (2)) were determined in the linear region, for small hexapod pitch and yaw rotations, and are summarized in Tab. 1. The off-diagonal elements are more than 100 times smaller than the diagonal elements, which corresponds to a misalignment between hexapod coordinates (shown in Fig. 2) and QPD orientation of less than 2°. The diagonal elements of M1, M2 are slightly larger than estimated by Eq. (4). The biggest deviation occurs for M1_{22}, which is 1.15 times larger than the simulated value $\text{M1}_{22}^{\text{sim}}$, but this is still within the expected parameter tolerances.

The heterodyne efficiency of the interfering beams on the four QPD1 segments that was also

Table 1. Measured DWS transfer matrices M1, M2 for QPD1, QPD2, respectively, which relate relative geometric wavefront tilts between LO beam and RX beam to DWS signals, cf. Eq. (2). Units are rad/rad.

Transfer matrix element	11	12	21	22
M1	16,000	-200	-300	-18,000
M2	16,400	-100	100	-16,000

recorded during the calibrated hexapod rotations is displayed in Fig. 7. The average of the maximum heterodyne efficiency values for each of the four quadrants is (58 ± 6) %, which agrees well with the simulation result from Eq. (5).

Unlike in the simulation result, Fig. 5, the position of the heterodyne efficiency maxima in Fig. 7 is different for each of the four quadrants by as much as ± 45 µrad. Our simulations have shown that this can be caused by wavefront curvature differences between LO beam and RX

#217032 - $15.00 USD Received 15 Jul 2014; revised 29 Aug 2014; accepted 29 Aug 2014; published 25 Sep 2014
(C) 2014 OSA

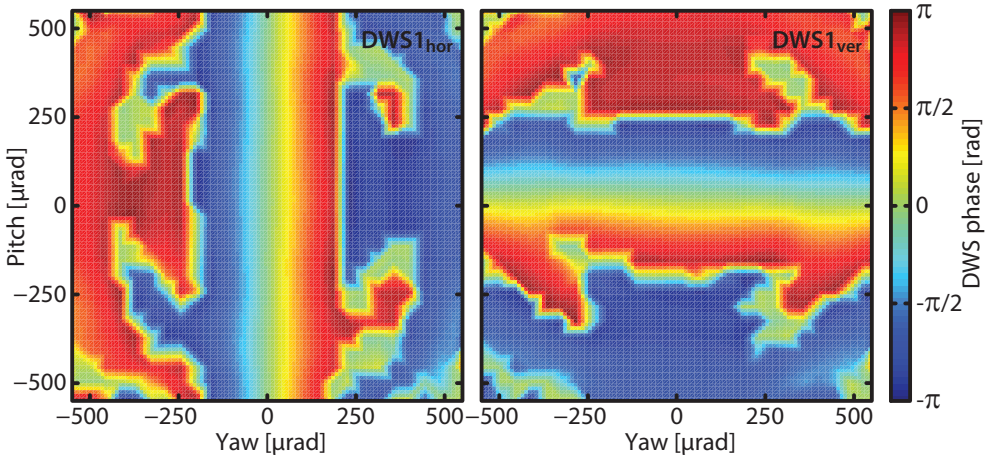

Fig. 6. DWS signals $DWS1_{hor}$ (left) and $DWS1_{ver}$ (right) measured with QPD1, while the hexapod performs calibrated pitch and yaw rotations.

beam of 0.01 /m, which agrees well with the alignment tolerances of LO beam generator and RX beam generator (cf. Sec. 2).

3.3. Measurement of beam coaligment during steering mirror closed-loop operation

Since satellilte pointing stability is expected to be improved for GRACE Follow-On compared to GRACE, we use a GRACE satellite pointing time series as a "worst case" to test the OBBM beam steering method with the setup in Fig. 2. Satellite pointing angles (roll, pitch, yaw) with respect to the line-of-sight were derived from the GRACE Level-1B RL02 data (available at [28, 29]) for a 12 h time series of January 1, 2008 [30]. The original 0.2 Hz data was interpolated to 1 Hz. The rotations as commanded to the hexapod are shown in Fig. 8 (top). The center of the OBBM aperture was chosen as nominal pivot to remain at the same transversal position of the RX beam during rotations.

The time series of LO beam and RX beam coalignment as obtained from the out-of-loop DWS measurement with QPD2 is shown in Fig. 8 (bottom), the linear power spectral density in Fig. 9. The DWS signals $DWS2_{hor}$ and $DWS2_{ver}$ have been converted to relative geometric wavefront tilt angles using the DWS transfer matrix M2 from Tab. 1. The measurement shows that the presented GRACE Follow-On beam steering method achieves LO beam and RX beam coalignment of better than 10 µrad with a stability of 10 µrad/$\sqrt{\text{Hz}}$ in the GRACE Follow-On frequency band of 0.002...0.1 Hz, as requested in Sec. 2.4. Only for frequencies between 0.002...0.0024 Hz, the horizontal beam coalignment stability is marginally above the requirement by less than 5 µrad/$\sqrt{\text{Hz}}$. However, with the RX beam being fixed, a physical beam coalignment jitter should manifest in the TX beam orientation as well, which is recorded by the differential position measurements TX_{hor}, TX_{ver}. Since for frequencies between 0.002...0.0024 Hz, the TX beam jitter is below 10 µrad/$\sqrt{\text{Hz}}$ for both TX_{hor} and TX_{ver}, we conclude that the beam coalignment stability requirement is fulfilled down to 0.002 Hz.

The time series of TX beam orientation TX_{hor}, TX_{ver} is displayed in Fig. 8 (bottom). The TX beam changes its orientation by less than $\pm$10 µrad under hexapod rotations of many mrad, which is a beam jitter suppression of almost three orders of magnitude.

For completeness, the linear power spectral density of the DWS measurements $DWS1_{hor}$ and $DWS1_{ver}$ of the in-loop quadrant photo diode QPD1 is also displayed in Fig. 9. The measure-

#217032 - $15.00 USD Received 15 Jul 2014; revised 29 Aug 2014; accepted 29 Aug 2014; published 25 Sep 2014
(C) 2014 OSA

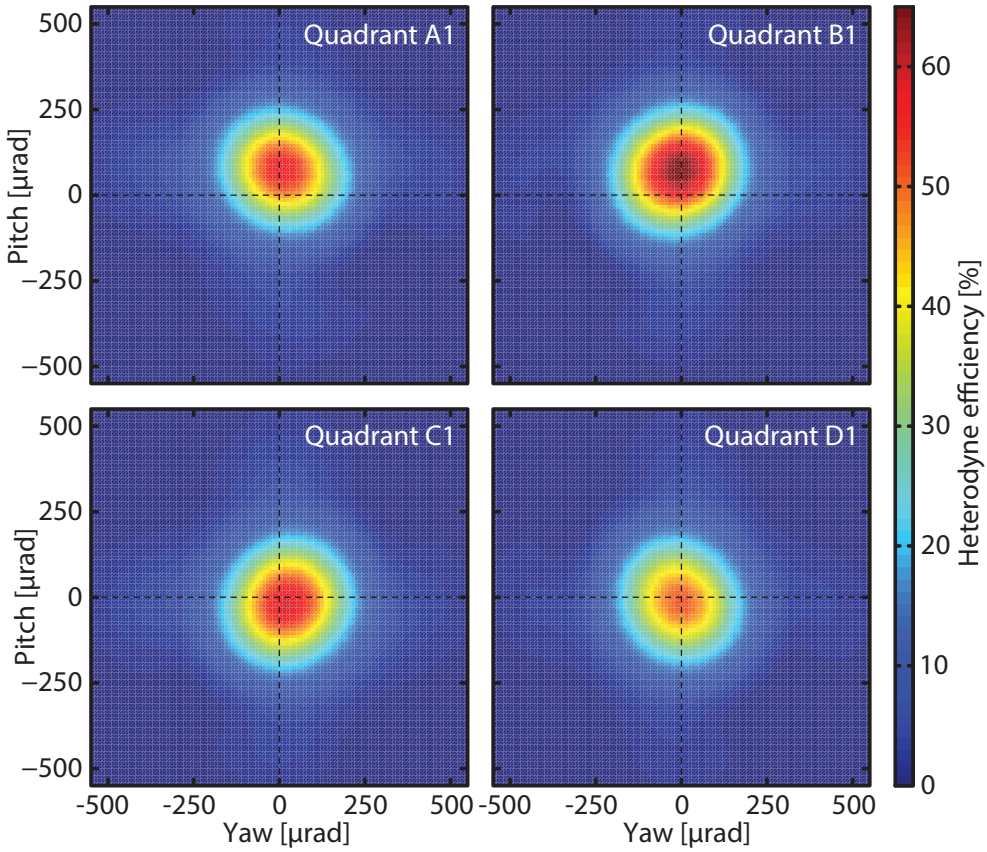

Fig. 7. Heterodyne efficiencies measured with the four quadrants A1, B1, C1, D1 of QPD1 while the hexapod performs calibrated pitch and yaw rotations.

ments are converted using DWS transfer matrix M1 from Tab. 1, leading to corresponding relative geometric wavefront tilt angles of below 0.01 µrad. Yet this is not a physical LO beam and RX beam coalignment, but only demonstrates the in-loop suppression.

3.4. Measurement of rotation-to-pathlength coupling

We have investigated rotation-to-pathlength coupling of the OBBM system shown in Fig. 2 while the steering mirror loop was closed. During hexapod roll, pitch, and yaw rotations of ± 2.5 mrad, we have determined pathlength deviations from the difference between phase changes on QPD1 (coherent sum of all four quadrants) and phase changes on PD-REF. The OBBM aperture center was chosen as nominal rotation pivot.

For hexapod roll, pitch, and yaw rotations, we have found coupling factors of 1 nm/mrad, 16 nm/mrad, and 13 nm/mrad, respectively, which fulfills the ranging error budget given in Sec. 2.5.

4. Conclusion

We have successfully implemented the GRACE Follow-On beam steering method on breadboard level and shown the operation of MHz Differential Wavefront Sensing beam steering while imitating realistic local spacecraft attitude jitter of many mrad taken from the GRACE

#217032 - $15.00 USD Received 15 Jul 2014; revised 29 Aug 2014; accepted 29 Aug 2014; published 25 Sep 2014
(C) 2014 OSA

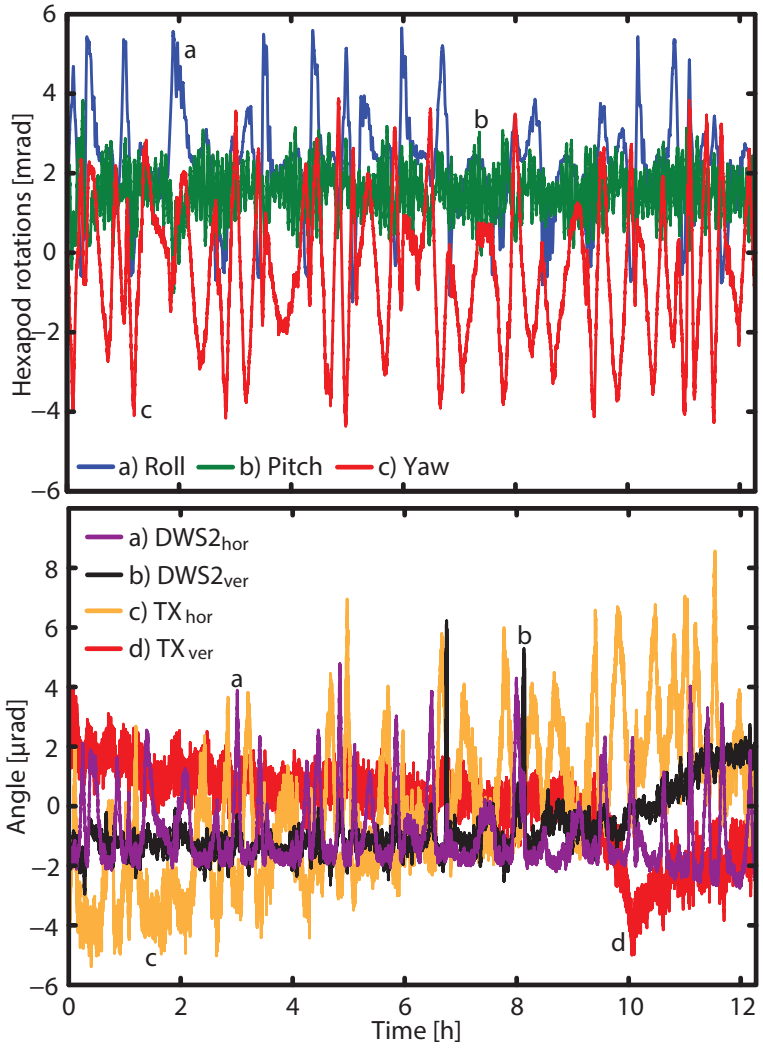

Fig. 8. Top: The hexapod performs rotations according to a GRACE satellite attitude jitter dataset, while the steering mirror loop is closed. Shown are hexapod commands, which are executed by the hexapod within $\pm 6\,\mu$rad by the manufacturer's specifications. Bottom: Coalignment of LO beam and RX beam during hexapod rotations obtained from the DWS signals $DWS2_{hor}$ and $DWS2_{ver}$ of the out-of-loop quadrant photo diode QPD2. DWS signals have been converted to relative geometric wavefront tilt angles using the DWS transfer matrix M2 from Tab. 1. Furthermore, orientation changes TX_{hor}, TX_{ver} of the TX beam are recorded with the differential position measurement of QPD3, QPD4.

#217032 - $15.00 USD Received 15 Jul 2014; revised 29 Aug 2014; accepted 29 Aug 2014; published 25 Sep 2014
(C) 2014 OSA

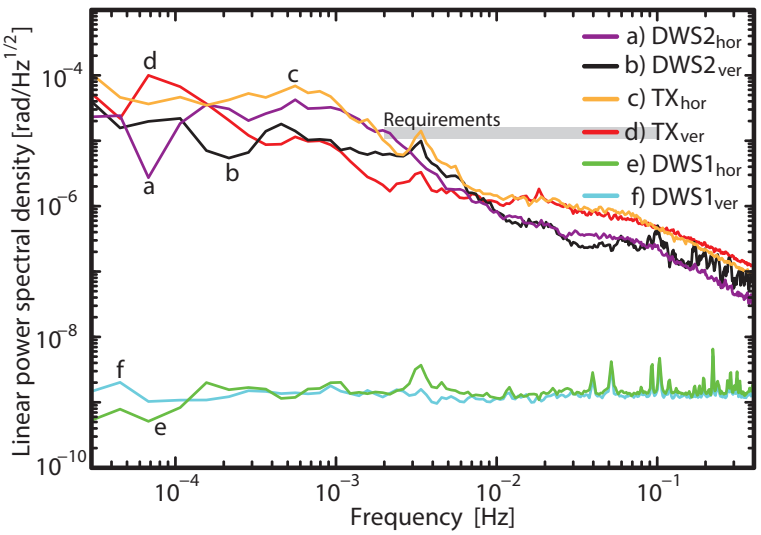

Fig. 9. Linear power spectral density of coalignment of LO beam and RX beam, while the hexapod performs rotations according to Fig. 8 (top). Both DWS signals DWS2$_{hor}$ and DWS2$_{ver}$ of the out-of-loop quadrant photo diode QPD2 have been converted to relative geometric wavefront tilt angles using the DWS transfer matrix M2 from Tab. 1. Furthermore, orientation changes TX$_{hor}$, TX$_{ver}$ of the TX beam are recorded with the differential position measurement of QPD3, QPD4. For completeness, the DWS measurements DWS1$_{hor}$ and DWS1$_{ver}$ of the in-loop quadrant photo diode QPD1 are also shown, converted to corresponding relative geometric wavefront tilt angles using DWS transfer matrix M1 from Tab. 1. Yet the DWS measurement of QPD1 is inherently small due to the in-loop suppression and does not imply a corresponding beam coalignment.

satellite mission with a hexapod.

We have verified that the proposed beam steering method is capable of maintaining an intersatellite laser interferometer link with beam pointing error of less than 10 µrad and stability of 10 µrad/$\sqrt{\text{Hz}}$ at 0.002...0.1 Hz. Furthermore, rotation-to-pathlength coupling of the beam steering setup was shown to be 1 nm/mrad for roll and below 20 nm/mrad for pitch and yaw rotations.

Acknowledgments

We would like to thank the “Deutsches Zentrum für Luft- und Raumfahrt” (DLR) for kindly providing the Elegant Breadboard Model of the GRACE Follow-On quadrant photo receiver. This work was partly funded by the “Bundesministerium für Bildung und Forschung” (BMBF, project number: 03F0654B) and by the “Deutsche Forschungsgemeinschaft” (DFG) within the Cluster of Excellence QUEST (Centre for Quantum Engineering and Space-Time Research).

#217032 - $15.00 USD Received 15 Jul 2014; revised 29 Aug 2014; accepted 29 Aug 2014; published 25 Sep 2014
(C) 2014 OSA